

## Transition zone in constant pressure converging flows

Article (Published Version)

Vasudevan, K P and Dey, J (2000) Transition zone in constant pressure converging flows. *Current Science*, 79 (6). pp. 821-828. ISSN 0011-3891

This version is available from Sussex Research Online: <http://sro.sussex.ac.uk/id/eprint/39906/>

This document is made available in accordance with publisher policies and may differ from the published version or from the version of record. If you wish to cite this item you are advised to consult the publisher's version. Please see the URL above for details on accessing the published version.

### **Copyright and reuse:**

Sussex Research Online is a digital repository of the research output of the University.

Copyright and all moral rights to the version of the paper presented here belong to the individual author(s) and/or other copyright owners. To the extent reasonable and practicable, the material made available in SRO has been checked for eligibility before being made available.

Copies of full text items generally can be reproduced, displayed or performed and given to third parties in any format or medium for personal research or study, educational, or not-for-profit purposes without prior permission or charge, provided that the authors, title and full bibliographic details are credited, a hyperlink and/or URL is given for the original metadata page and the content is not changed in any way.

# Transition zone in constant pressure converging flows

K. P. Vasudevan and J. Dey\*

Department of Aerospace Engineering, Indian Institute of Science, Bangalore 560 012, India

**The effect of lateral streamline convergence alone on the transitional flow characteristics has been studied towards modelling the transition zone. Apart from a thicker boundary layer, the transitional flow characteristics are found to be similar to those in two-dimensional constant pressure flows. The transition zone has been modeled using the linear-combination model for two-dimensional flows.**

## Introduction

It is now a well-accepted fact that the problem of laminar-turbulent transition in viscous flows is one of the most challenging ones in fluid dynamics today. Consequently, transition zone modelling remains a critical phase in the prediction of viscous flow past bodies<sup>1</sup>. For example, the transition region in a gas turbine blade can be as much as 80% of the blade surface<sup>2</sup> and so requires careful design consideration, as the peak heat transfer rate occurs within this region. The most disquieting aspect about transition is that there is no unique route to transition. Also, parameters like the pressure gradient, streamline convergence/divergence, streamline curvature (longitudinal/lateral), all acting simultaneously or individually, influence the transition process, thus making our understanding of the process more difficult.

Although there is no unique route to transition, the spot-wise transition theory of Emmons<sup>3</sup> provides a reasonable explanation for a large class of boundary layer transitional flows. According to this theory, flow breakdown occurs via the appearance of turbulent spots, which then propagate downstream, making the flow intermittent in nature (with the laminar intervals slowly disappearing) and the flow finally attains a fully turbulent state, further downstream. Narasimha<sup>4</sup> in proposing the hypothesis of *concentrated breakdown* suggested that the flow breakdown occurs at a fixed stream-wise location ( $x_i$ ), called the 'onset of transition'. Thus a finite transition zone length exists between the onset of transition and the fully turbulent state. Though the overall process of transition may be gradual, the onset of transition may be relatively sudden<sup>5</sup>. A measure of

the extent of turbulent region in transitional flow is the 'fraction of time for which the flow remains turbulent' at any streamwise station. This is given by the intermittency factor ( $\gamma$ ). Various  $\gamma$ -distributions have been proposed in the past for two-dimensional (2-D) flows<sup>4,6,7</sup>. Similarly, a variety of transition zone models are now available<sup>8</sup>.

Most of the earlier works on the transition zone were undertaken with 2-D mean flows<sup>8</sup>. But three-dimensional flows are more important as they are frequently encountered. However, these flows are complex owing to the presence of many parameters like the pressure gradient, streamline curvature (lateral and longitudinal), streamline convergence/divergence, etc. For a better understanding and modelling of the transition zone, we need to have enough knowledge on the effect of each of these parameters individually on the transitional flow characteristics. Among the various flow parameters affecting the transitional flow characteristics, the effect of pressure gradient (favourable and adverse) has already been studied<sup>6,9-13</sup>. Kohama<sup>14</sup> has investigated the effect of curvature on a concave wall. Streamline convergence/divergence causes an additional strain rate and is known to produce a large effect on turbulent boundary layer growth, and is likely to affect transition characteristics as well. Studies carried out on internal flows in turbo-machines show<sup>15</sup> that the start and length of transition are affected by the presence of lateral convergence and divergence to a far greater degree than by pressure gradient alone. Recently, Saddoughi and Joubert<sup>16</sup> and Panchapakesan *et al.*<sup>17</sup> have investigated laterally strained turbulent boundary layers. While a significant reduction of the skin friction and a thicker boundary layer, compared to 2-D flows, have been observed by Panchapakesan *et al.*<sup>17</sup> for converging flows, Saddoughi and Joubert<sup>16</sup> find a thinner boundary layer and increased skin friction in a laterally diverging flow. Also, a considerable reduction in the Reynolds stresses in the inner region and an increase in the turbulent kinetic energy in the outer part of the flow have been reported<sup>17</sup>, along with the result that the mean velocity profile is similar to that in a 2-D adverse pressure gradient flow. Furthermore, in terms of a newly-defined convergence/divergence parameter<sup>17</sup>, a diverging flow attains equilibrium while this is not so for converging flows. One may therefore expect some effect of streamline convergence on transitional flows also. In this pa-

\*For correspondence. (e-mail: jd@aero.iisc.ernet.in)

One of the earliest and best-known transition zone models has emerged from the transition studies initiated by Prof. S. Dhawan at IISc. This paper, which has reference to this models, is dedicated to Prof. Dhawan on his 80th birthday.

per we present the results of our investigations on the effect of lateral streamline convergence on the transitional flow characteristics towards modelling the transition zone. Ramesh<sup>18</sup> has studied the transition zone with streamline divergence. The main result of the investigation is that a constant pressure diverging flow bears many similarities with the corresponding 2-D flow.

## Experimental details

All the experiments reported here were carried out in the Low Turbulence Wind Tunnel ( $\approx 0.03\%$  free stream turbulence level) in the Department of Aerospace Engineering. The contraction ratio of the tunnel is 14:1. A thyristor controlled induction motor drive is used to maintain the motor rpm to within 0.5% of the desired rpm. The maximum flow velocity obtainable in this tunnel is 25 m/s.

In order to study the transitional flow characteristics under converging streamlines, the square test section has been modified. As shown schematically in Figure 1, a constant pressure converging flow is achieved by converging the tunnel side-walls at  $10^\circ$  and diverging the roof. A highly-polished aluminum plate (200 mm  $\times$  500 mm) forms one side of the converging channel, and the boundary layer measurements are made on this plate (see Figure 1);  $x$  is the stream-wise coordinate,  $y$  is the coordinate normal to the plate, and  $z$  is the span-wise coordinate. The plate has a super-elliptical leading edge to ensure attached flow over the plate<sup>19</sup>. In order to have a thicker boundary layer in the test section, the converging section is preceded by a flat section of  $0 \leq x \leq 8$  cm (see Figure 1). In the experiment of Ramesh<sup>18</sup>, the flow divergence was achieved by diverging the side walls and converging the roof. We have selected the half angle of convergence to be  $10^\circ$  (see Figure 1), as this is approximately the same as the half angle of the spot envelope. The divergence angle in the experiment of Ramesh was also about  $10^\circ$ . As the original square test section has been replaced by a converging channel for the present study, an additional contraction, based on the proposal of Ramaseshan and Ramaswamy<sup>20</sup>, has to be provided for smooth entry of the flow into the test section (see Figure 1).

A constant-temperature hot-wire anemometer (Sunshine Industries Model No. 717) with 5  $\mu$ m diameter Platinum-Rhodium alloy Wollaston process wire as the sensing element (having length to diameter ratio of 800) has been used. The probe is calibrated before each experiment.

Artificial turbulent spots are generated by a loud speaker providing sufficiently strong air pulses through a 0.5 mm hole located on the flat plate at  $x_s = 135$  mm downstream of the leading edge and on the line of symmetry ( $z = 0$ ).

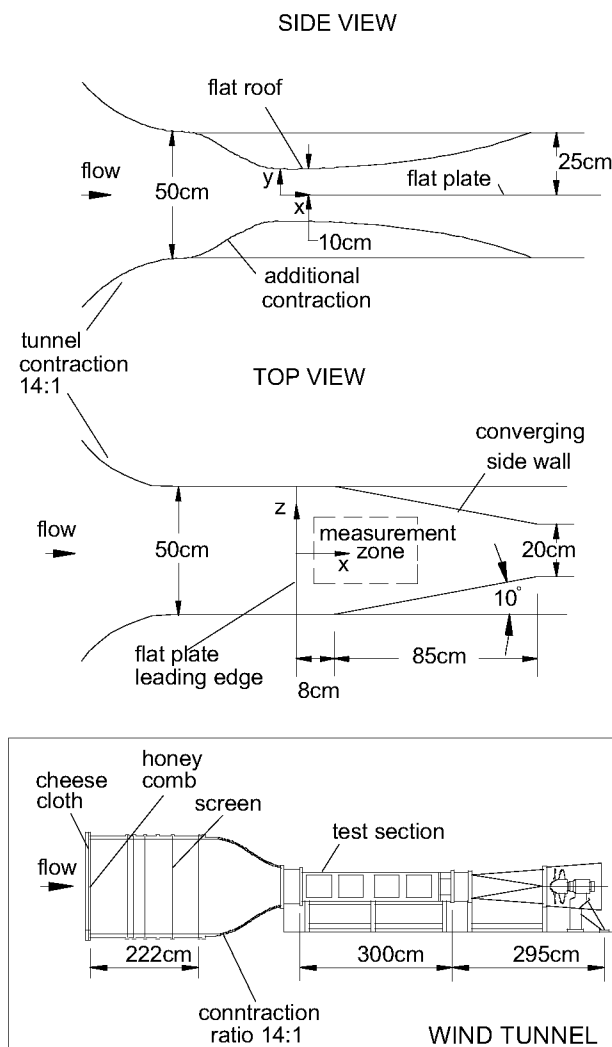


Figure 1. Schematic of the flow geometry.

The sampling time for all the measurements has been fixed at 10 s. The sampling rate or the frequency of data acquisition is 2 kHz, i.e. each sampled data set contains 20000 data points.

The measured stream-wise pressure distribution inside the test section is shown in Figure 2 in terms of the coefficient of pressure ( $C_p$ ),

$$C_p = 1 - \left( \frac{U}{U_R} \right)^2, \quad (1)$$

where  $U_R$  is the reference free-stream velocity at  $x = 100$  mm from the flat plate leading edge. It can be seen that the pressure (and also  $U$ ) is constant in the test section; the jump in  $C_p$  at the leading edge may be due to the contraction profile slightly extending into the flat roof region. Similarly, the span-wise pressure distribution is found to be nearly constant<sup>21</sup>.

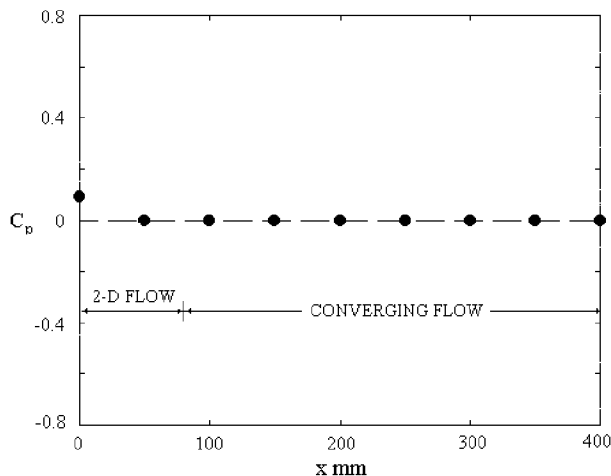


Figure 2. Stream-wise variation of  $C_p$ .

## Results and discussion

Both the laminar and transitional boundary layer flows have been investigated. In addition, the propagation characteristics of an artificially-generated turbulent spot are examined. All the measurements reported here are carried out corresponding to a free-stream velocity of  $U = 10.3$  m/s.

### Laminar flow

The laminar boundary layer measurements have been made both in the 2-D region ( $0 \leq x \leq 80$  mm) and in the converging section at various stream-wise locations along the line of symmetry. The normalized velocity profiles ( $u_L/U$ ) are compared with the Blasius profile for 2-D constant pressure flow<sup>22</sup> in Figure 3 (for the sake of clarity, the velocity profiles are shown for five  $x$ -locations); here (and hereafter) the subscript  $L$  denotes the laminar condition. It can be seen that the measured velocity profiles in the converging section are close to the Blasius profile. The investigation by Ramesh<sup>18</sup> also shows that the laminar velocity profiles in a constant pressure diverging flow is the Blasius one but with a thinner boundary layer. The stream-wise variation of the momentum thickness ( $\theta_L$ ) and the shape parameter ( $H_L$ ) are shown in Figure 4. It can be seen that in the 2-D region ( $0 \leq x \leq 80$  mm), the measured  $\theta_L$  agrees well with the Blasius values (Figure 4). In the converging flow region ( $80 \leq x \leq 400$  mm),  $\theta_L$  values are higher than the corresponding Blasius values (Figure 4), thus indicating a thickening effect on the boundary layer. This thickening effect can be attributed to the streamline convergence. The shape factor has a constant value of  $H_L \approx 2.6$  (Figure 4) corresponding to the Blasius value. This has to be so since the velocity profiles are of similar shape at all these locations<sup>23</sup>.

Apart from the thickening effect, the observed similarity with the Blasius flow is expected due to the similarity between a converging/diverging boundary layer flow and a 2-D flow shown by Ramesh *et al.*<sup>24</sup>. Following Kehl<sup>25</sup>, a diverging/converging flow can be approximated by a source/sink flow, as shown in Figure 5. Let  $u$ ,  $v$ , and  $w$  be the velocity components in the  $x$ ,  $y$  and  $z$  directions, respectively. The span-wise velocity ( $w$ ) is taken as

$$w = uz/(a + x).$$

For the coordinate system shown in Figure 5,  $w = 0$  along  $z = 0$  (i.e. on a streamline), but

$$\left( \frac{\partial w}{\partial z} \right)_{z=0} \neq 0.$$

This non-zero component causes the extra lateral strain rate. The governing equations under the boundary layer approximation are<sup>22</sup>,

$$\frac{\partial u}{\partial x} + \frac{\partial v}{\partial y} + \frac{\partial w}{\partial z} = \frac{\partial u}{\partial x} + \frac{\partial v}{\partial y} + \frac{u}{a+x} = 0, \quad (2)$$

$$u \frac{\partial u}{\partial x} + v \frac{\partial u}{\partial y} = -\frac{1}{\rho} \frac{\partial p}{\partial x} + \nu \frac{\partial^2 u}{\partial y^2},$$

$$-\frac{1}{\rho} \frac{\partial p}{\partial x} = U \frac{dU}{dx}. \quad (3)$$

The boundary conditions are  $u = v = 0$  at  $y = 0$ ,  $u \rightarrow U$  as  $y \rightarrow \infty$ .

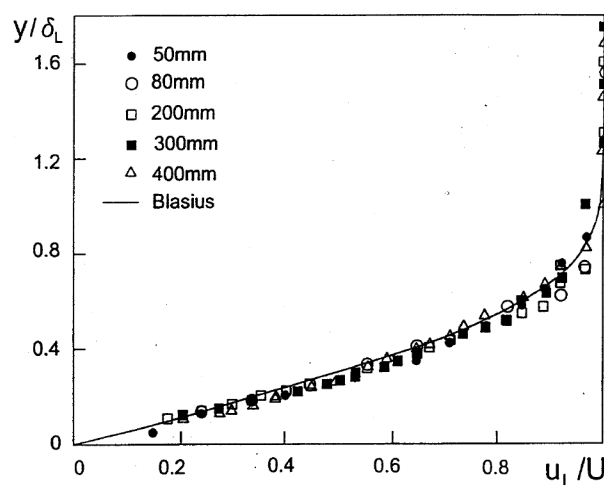
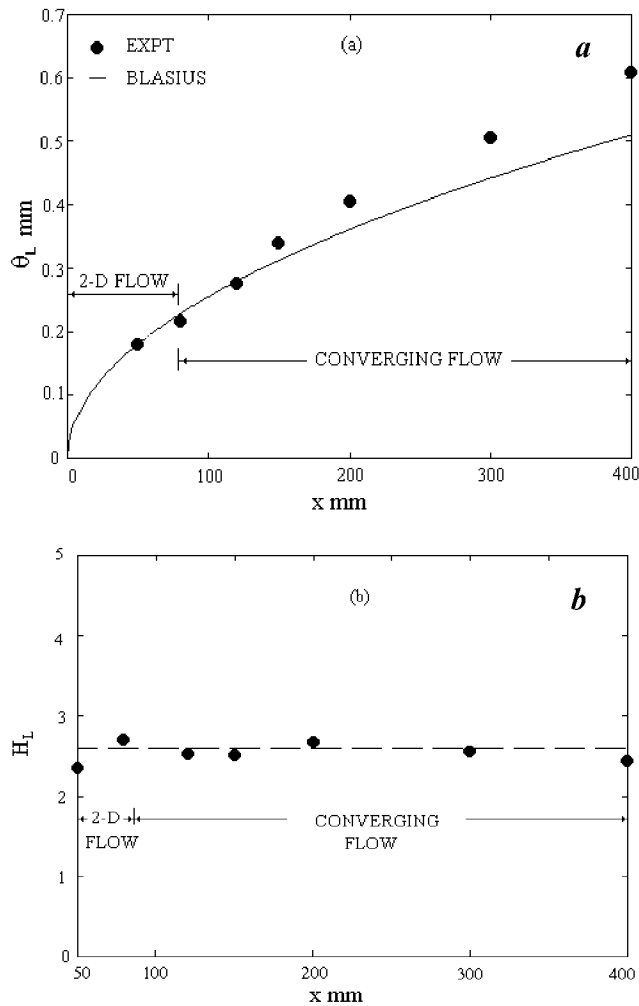
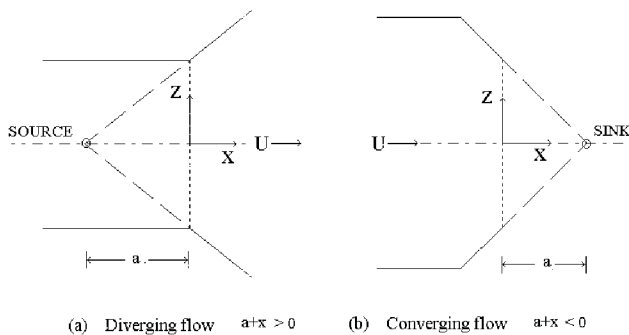


Figure 3. Comparison of the measured laminar velocity profiles with Blasius profile.



**Figure 4.** Stream-wise variation of the laminar momentum thickness (a) and laminar shape factor (b).



**Figure 5.** Source/sink approximation of diverging/converging flow.

Ramesh *et al.*<sup>24</sup> have shown that the Mangler type transformation,

$$X = \frac{(a+x)^3}{3a^2}, \quad Y = \left(\frac{a+x}{a}\right)y \quad (4)$$

$$u \rightarrow U_1, \quad V_1 \rightarrow \frac{a}{a+x} \left[ v + \frac{yu}{a+x} \right], \quad U \rightarrow U_{1\infty},$$

reduces eqs (2) and (3) to 2-D flows; although Ramesh *et al.*<sup>24</sup> have extended the Mangler transformation to turbulent flows, only the laminar flow is considered here for the sake of simplicity. A straight-forward reduction of (2) and (3) to the Falkner–Skan equations is also possible by means of the following transformations<sup>26</sup>. The velocity scaling,

$$u \rightarrow U_2 \left( \frac{a}{a+x} \right), \quad v \rightarrow V_2 \left( \frac{a}{a+x} \right),$$

$$u_\infty \rightarrow U_{2\infty} \left( \frac{a}{a+x} \right) \quad (5)$$

reduces (2) and (3) to

$$\frac{\partial U_2}{\partial x} + \frac{\partial V_2}{\partial y} = 0, \quad (6)$$

$$U_2 \frac{\partial U_2}{\partial x} - \frac{U_2^2}{(a+x)} + V_2 \frac{\partial U_2}{\partial y} = U_{2\infty} \frac{dU_{2\infty}}{dx} - \frac{U_{2\infty}^2}{(a+x)} + v \left( \frac{a+x}{a} \right) \frac{\partial^2 U_2}{\partial y^2}, \quad (7)$$

respectively. Using the similarity variables<sup>26</sup>,

$$\eta = y \left[ \frac{U_{2\infty}(1+m)}{v(a+x)} \right]^{\frac{1}{2}} \left( \frac{a}{a+x} \right)^{\frac{1}{2}},$$

$$\Psi = \left[ \frac{U_{2\infty}v(a+x)}{(1+m)} \right]^{\frac{1}{2}} \left( \frac{a+x}{a} \right)^{\frac{1}{2}} F(\eta), \quad (8)$$

(6) and (7) reduce to the Falkner–Skan similarity equation<sup>26</sup>,

$$\left( \frac{m-1}{m+1} \right) (F'^2 - 1) - \frac{1}{2} FF' = F''', \quad (9)$$

under the condition  $U_{2\infty} = K(a+x)^m$ , where  $K$  is a constant; the stream function  $\psi$  is such that  $U_2 = \partial\psi/\partial y$  and  $V_2 = -\partial\psi/\partial x$ . The choice  $m = 1$  gives the Blasius solution. The above transformation shows that the velocity scaling (5) is essential for reduction to 2-D flows. Therefore, the observed similarity with the Blasius flow is not surprising.

### Transitional flow

Transition is initiated with the help of a grid with a  $1\text{ cm} \times 1\text{ cm}$  mesh (of 3 mm circular rods). The grid is so fixed that the entire transition zone is within the measurement region.

The intermittency distribution in the transition zone is measured by the method employed by Ramesh *et al.*<sup>27</sup>. In this method, the signal is double differentiated and then squared to sensitize it. A probability distribution plot of the sensitized signal is then obtained, which in turn provides a threshold to distinguish between the turbulent and non-turbulent parts of the signal. The sensitized signal is averaged over a time scale of 5 sample points (0.0025 s) to ensure better congruity of the intermittency function with the sensitized signal. This scale is of the order of the Kolmogorov length scale<sup>28</sup>. The intermittency distribution along the longitudinal line of symmetry has been measured at various stream-wise locations ( $x = 150, 200, 250, 300, 350, 400, 450, 500, 550, 600\text{ mm}$ ) with the hot-wire probe kept at a height of 0.5 mm with respect to the flat plate. The measured  $\gamma$ -distribution in the transition zone is compared with the universal 2-D constant pressure law of Narasimha<sup>4</sup>,

$$\gamma = 1 - e^{-0.4\zeta^2}, \quad \zeta = (x - x_t)/\lambda, \quad (10)$$

in Figure 6. Here  $x_t$  is the transition onset location, and  $\lambda = ([x]_{\gamma=0.75} - [x]_{\gamma=0.25})$  is a measure of the transition zone length. It can be seen that the  $\gamma$ -distribution follows the 2-D universal law. This is indeed a very interesting result, as the 2-D  $\gamma$ -distribution can be used in a flow with streamline convergence. The  $\gamma$ -distribution in a diverging flow is also found to follow the same 2-D law, as reported by Ramesh *et al.*<sup>27</sup>.

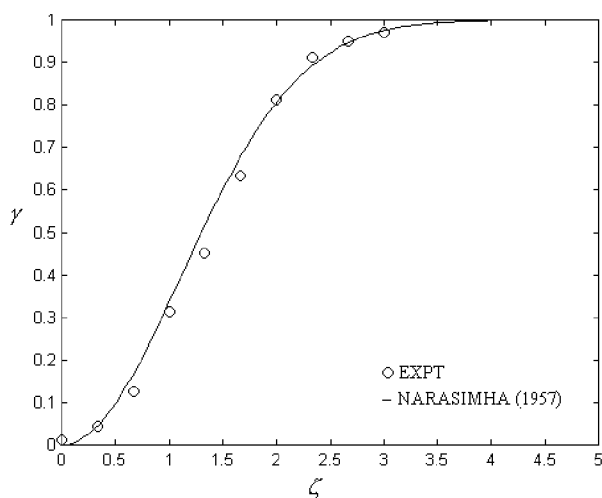


**Figure 6.** Comparison of the measured intermittency distribution with 2-D distribution.

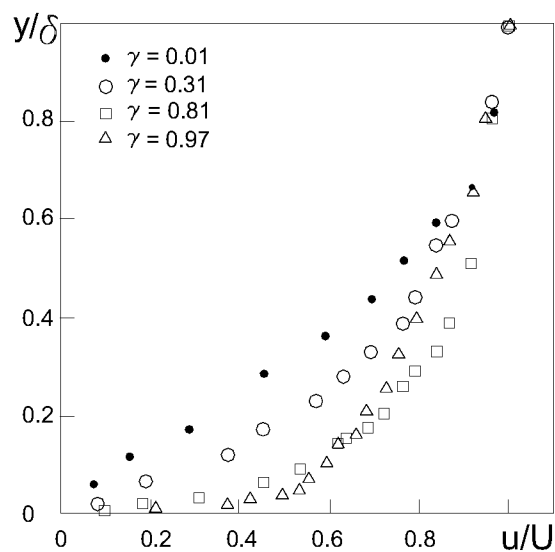


**Figure 7.** Transitional velocity profiles.

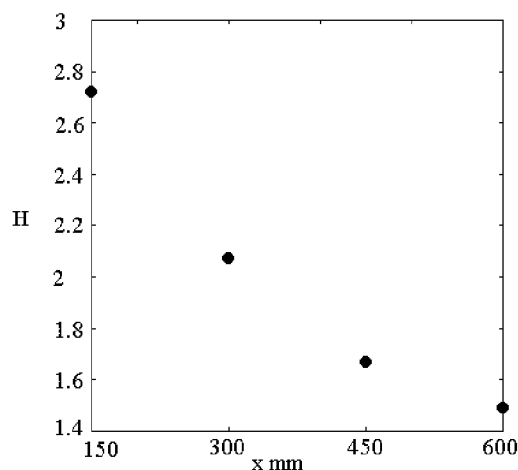


**Figure 8.** Variation of the shape-factor in the transition zone.

The measured transitional velocity profiles at various stream-wise locations ( $x = 150, 300, 450, 600\text{ mm}$ ) along the longitudinal line of symmetry are shown in Figure 7. At the  $x$ -location where the intermittency is only 1%, the velocity profile is very similar to that for a laminar flow. As one goes downstream,  $\gamma$  increases and the velocity profiles become fuller, thus indicating a turbulent flow development. This is expected since, at the beginning of the transition zone, the flow is nearly laminar and is fully turbulent at the end of transition zone. It can be seen in Figure 8 that the shape factor changes from the near-laminar value (of  $H \approx 2.7$ , at  $\gamma = 0.01$ ) to the nearly fully turbulent value (of  $H \approx 1.5$ , at  $\gamma = 0.97$ ) within the transition zone. Interestingly, these values are similar to those for the 2-D transitional flow over a flat plate<sup>22,29</sup>.

As mentioned earlier, many transition zone models are now available<sup>8</sup>. We have used the Linear-Combination Model (LCM) of Dhawan and Nara-

simha<sup>30</sup>, as it is simple and still very effective in predicting various transitional boundary layer parameters. This model takes the mean velocity profile in the transition zone as a linear combination of the laminar and the turbulent profiles, weighted by the flow intermittency,

$$\frac{u}{U} = \frac{u_L}{U}(1-\gamma) + \frac{u_T}{U}\gamma. \quad (11)$$

Here (and hereafter) the subscript T denotes the turbulent value. This model assumes<sup>8</sup> that the laminar boundary layer originates at the leading edge of the flat plate, and the turbulent boundary layer originates at the transition onset location  $x_t$ . Apart from the simplicity associated with the LCM of Dhawan and Narasimha<sup>30</sup>, the momentum imbalance of this model is small<sup>31</sup>. Interestingly, among the other models in this class, the momentum balance aspect is known only for this model. Briefly, for the velocity distribution (11), the expression for the momentum thickness used by Dhawan and Narasimha<sup>30</sup> is,

$$\theta = \gamma(1-\gamma) \int_0^\delta [\overline{u_L} - (1-\overline{u_T}) + \overline{u_T} - (1-\overline{u_L})] dy + (1-\gamma)^2 \theta_L + \gamma^2 \theta_T. \quad (12)$$

Here  $\overline{u_L}$  and  $\overline{u_T}$  are non-dimensional. With this expression for  $\theta$ , it is slightly difficult to estimate the momentum imbalance although not impossible. However, a simpler expression<sup>31</sup> for  $\theta$  that also follows from the velocity distribution (11),

$$\theta = (1-\gamma)\theta_L + \gamma\theta_T + \gamma(1-\gamma) \int_0^\delta (\overline{u_L} - \overline{u_T})^2 dy, \quad (13)$$

makes it easier to estimate the momentum imbalance from the momentum integral equation for constant pressure flows,

$$2 \frac{d\theta}{dx} - C_f = 2 \left( I_1 + \frac{dI_2}{dx} \right), \quad (14)$$

$$I_1 \equiv \frac{d\gamma}{dx} (\theta_T - \theta_L), \quad I_2 \equiv \gamma(1-\gamma) \int_0^\delta (\overline{u_L} - \overline{u_T})^2 dy.$$

Here, following the velocity distribution (11), the skin friction coefficient ( $C_f$ ) also is a linear combination type, i.e.  $C_f = (1-\gamma)C_{fL} + \gamma C_{fT}$ . As shown in Figure 9, the momentum residual ( $I_1 + dI_2/dx$ ) is small compared to  $d\theta/dx$ ;  $I_1$  and  $dI_2/dx$  are of opposite signs and tend to cancel each other<sup>31</sup>; the data of Schubauer and Klebanoff<sup>29</sup> are used to estimate these quantities. This fact and the associated simplicity of the model render it an attractive one.

For the present transition zone model, the laminar profile is the Blasius profile, as mentioned earlier. Although a log plus wake profile is desirable for turbulent profiles, the wake parameter is not fully defined for low Reynolds number flows<sup>32</sup>. As such, we have used a simple power law velocity profile,

$$\frac{u_T}{U} = \left( \frac{y}{\delta_T} \right)^{\frac{1}{n}}, \quad (15)$$

where  $\delta_T$  is the turbulent boundary layer thickness. The value of the exponent  $n$  varies between 5 and 8, depending on the flow Reynolds number. In the present analysis,  $n = 7$  is taken, as it is found that the measured velocity profile is in good agreement with the profiles predicted by LCM.  $\delta_T$  is obtained from the momentum integral equation for converging/diverging flows. Under the source/sink approximation of Kehl<sup>25</sup>, the momentum integral equation is

$$\frac{d\theta_T}{dx} + \frac{\theta_T}{a+x} = \frac{C_{fT}}{2}. \quad (16)$$

In order to solve (16), a correlation between  $C_{fT}$  and the Reynolds number ( $Re = Ux/\nu$ ) is built using the data of Panchapakesan *et al.*<sup>17</sup> for turbulent flow in a converging channel, as the range of the convergence parameter ( $D = 1/(a+x)$ ) in their experiment and in the present case is nearly same<sup>21</sup>. The correlation used is

$$C_f = 0.0084(Re)^{-0.0578}; \quad (17)$$

the number of data points is limited (only four). As shown in Figure 10, the measured transitional velocity

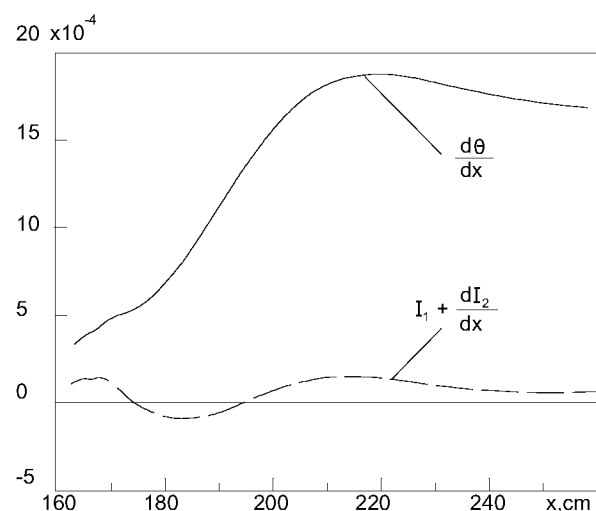


Figure 9. Momentum residual in comparison to the gradient of the momentum thickness in the transition zone.

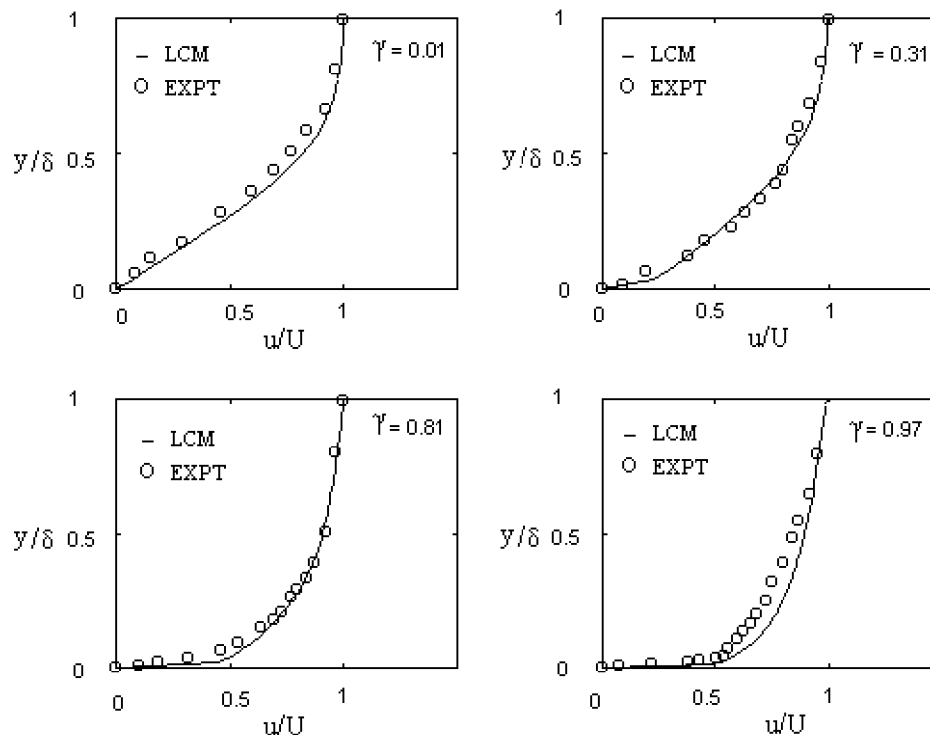


Figure 10. Comparison of the measured velocity profiles with the LCM prediction.

profiles can be predicted using the LCM. For diverging streamlines, Ramesh<sup>18</sup> reports that the same LCM adequately represents the transition zone. Thus a 2-D model can be used even in flows with converging/diverging streamlines.

The spot propagation characteristics of an artificial spot are also found to be similar to those in 2-D constant pressure flows<sup>33</sup> like, for example, the conical similarity of Cantwell *et al.*<sup>34</sup> shown in Figure 11; here  $x_c$  and  $z_c$  are the similarity co-ordinates.

## Conclusions

The effect of lateral streamline convergence alone on the transitional flow characteristics has been studied as part of the ongoing project at the Dept. of Aerospace Engineering, IISc, on transition zone modelling. A constant pressure lateral streamline convergence is achieved by converging the side-walls and appropriately diverging the roof; the half angle of convergence is chosen as  $10^\circ$ , which is approximately the same as the half of the turbulent spot envelope in constant pressure two-dimensional flows. The important findings of the present work are the following.

Except for a thicker boundary layer, the laminar boundary layer is of the Blasius type for 2-D constant pressure flows. The intermittency distribution in the transition zone follows the 2-D universal constant pressure law. The 2-D linear combination model for the

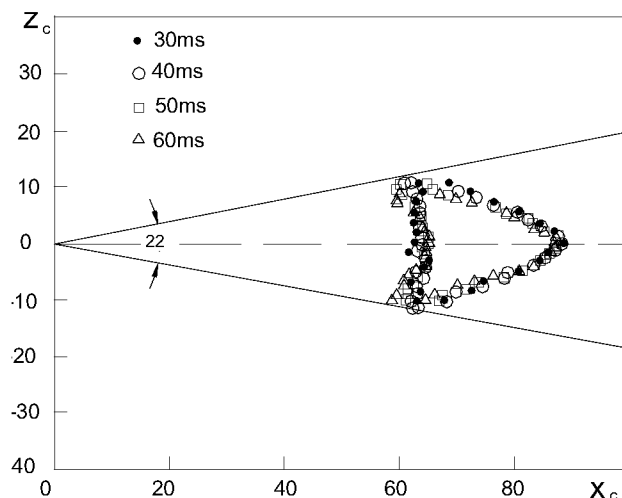


Figure 11. Conical similarity of turbulent spots.

transition zone has been found to be satisfactory in predicting transitional velocity profiles, even in converging streamline flows. The spot propagation characteristics are also similar to those in 2-D constant pressure flows.

To conclude, the present study shows that apart from causing a thicker boundary layer, the streamline convergence has a negligible effect on the transitional flow characteristics.

1. Cebeci, T., *Numerical and Physical Aspect of Aerodynamic Flows. II*, Springer Verlag, New York, 1983.
2. Turner, A. B., *J. Mech. Engg. Sci.*, 1971, **13**, 1–12.



3. Emmons, H. W., *J. Aeronaut. Sci.*, 1951, **18**, 490–498.
4. Narasimha, R., *J. Aero. Sci.*, 1957, **24**, 711–712.
5. Narasimha, R., *Prog. Aerospace Sci.*, 1985, **22**, 29–80.
6. Abu-Ghanam, B. J. and Shaw, R., *J. Mech. Engg. Sci.*, 1980, **22**, 213–228.
7. Arnal, D., AGARD-FDP-VKI cours special, 1986.
8. Narasimha, R. and Dey, J., *Sadhana*, 1989, **14**, 93–120.
9. Wygnanski, I., Proceedings of the International Conference Role of Coherent Structure in Modelling Turbulence & Mixing, Madrid, 1980.
10. Narasimha, R., Subramanian, C. and Badrinarayanan, M. A., *AIAA J.*, 1984, **22**, 837–839.
11. Narasimha, R., Devasia, K. J., Gururani, G. and Badrinarayanan, M. A., *Exp. Fluids*, 1984, **2**, 171–176.
12. Gostelow, J. P., Blunden, A. R. and Walker, G. J., ASME 92-Paper No. GT-380, 1992.
13. Van Hest, B. F. A., Ph D thesis, Delft University of Technology, Delft, 1996.
14. Kohama, Y., Proceedings of the IUTAM Symposium, Bangalore, 1988.
15. Potti, M. G. S. and Soundaranayagam, S., Proceedings of the Conference Boundary Layer Transition and Control, Cambridge, UK, 33.1–33.14, 1991.
16. Saddoughi, S. G. and Joubert, P. N., *J. Fluid Mech.*, 1991, **229**, 173–204.
17. Panchapakesan, N. R., Nickels, T. B., Joubert, P. N. and Smits, A. J., *J. Fluid Mech.*, 1997, **349**, 1–30.
18. Ramesh, O. N., Ph D thesis, Indian Institute of Science, Bangalore, 1997.
19. Prasad, S. N. and Narasimha, R., *Exp. Fluids*, 1994, **17**, 358–360.
20. Ramaseshan, S. and Ramaswamy, M. A., Proceedings of the 12th Australasian Fluid Mechanics Conference, University of Sydney, Australia, 1995.
21. Vasudevan, K. P., M Sc Engg. Thesis, Indian Institute of Science, Bangalore, 2000.
22. Schlichting, H., *Boundary Layer Theory*, McGraw Hill, 1960.
23. Rosenhead, L. (ed.), *Laminar Boundary Layers*, Clarendon Press, Oxford, 1962.
24. Ramesh, O. N., Dey, J. and Prabhu, A., *Zeit. Angew. Math. Phys.*, 1997, **48**, 694–698.
25. Kehl, A., see ref. 22.
26. Tyagi, O. P. and Dey, J., to appear.
27. Ramesh, O. N., Dey, J. and Prabhu, A., *Exp. Fluids*, 1996, **21**, 259–263.
28. Hedley, T. B. and Keffer, J. F., *J. Fluid Mech.*, 1974, **64**, 625–644.
29. Schubauer, G. B. and Klebanoff, P. S., NACA TN-3489, 1955.
30. Dhawan, S. and Narasimha, R., *J. Fluid. Mech.*, 1958, **3**, 418–437.
31. Dey, J., *Trans. ASME J. Turbomachinery*, 2000, **122**, 587–588.
32. Coles, D. and Barker, S. J., *Turbulent Mixing in Non-reactive and Reactive Flows* (ed. Murthy, S. N. B.), Plenum Press, New York, 1975, pp. 285–292.
33. Vasudevan, K. P., Dey, J. and Prabhu, A., *Exp. Fluids* (to appear).
34. Cantwell, B., Coles, D. and Dimotakis, P., *J. Fluid Mech.*, 1978, **87**, 641–672.

ACKNOWLEDGEMENT. We thank Prof. A. Prabhu for his invaluable support and various suggestions during the course of this work. The financial support from AR&DB through a project is gratefully acknowledged.